Biomedicine & Pharmacotherapy 175 (2024) 116674

Contents lists available at ScienceDirect

Biomedicine & Pharmacotherapy

journal homepage: www.elsevier.com/locate/biopha

MPoMA protects against lung epithelial cell injury via p65 degradation

Soheun Lee [1], Suh Jin Yoon [2], Ji Hyun Oh [3], Jae-Sang Ryu [4], Yunjeong Park [*,5], Eun Sook Hwang [**,6]

College of Pharmacy and Graduate School of Pharmaceutical Sciences, Ewha Womans University, Seoul 03760, Republic of Korea

ARTICLE INFO

Keywords:
AQ
IL-8
Lung epithelial cell damage
p65
MPoMA

ABSTRACT

Numerous cases of lung injury caused by viral infection were reported during the coronavirus disease-19 pandemic. While there have been significant efforts to develop drugs that block viral infection and spread, the development of drugs to reduce or reverse lung injury has been a lower priority. This study aimed to identify compounds from a library of compounds that prevent viral infection that could reduce and prevent lung epithelial cell damage. We investigated the cytotoxicity of the compounds, their activity in inhibiting viral spike protein binding to cells, and their activity in reducing IL-8 production in lung epithelial cells damaged by amodiaquine (AQ). We identified *N*-(4-(4-methoxyphenoxy)-3-methylphenyl)-*N*-methylacetamide (MPoMA) as a non-cytotoxic inhibitor against viral infection and AQ-induced cell damage. MPoMA inhibited the expression of IL-8, IL-6, IL-1β, and fibronectin induced by AQ and protected against AQ-induced morphological changes. However, MPoMA did not affect basal IL-8 expression in lung epithelial cells in the absence of AQ. Further mechanistic analysis confirmed that MPoMA selectively promoted the proteasomal degradation of inflammatory mediator p65, thereby reducing intracellular p65 expression and p65-mediated inflammatory responses. MPoMA exerted potent anti-inflammatory and protective functions in epithelial cells against LPS-induced acute lung injury *in vivo*. These findings suggest that MPoMA may have beneficial effects in suppressing viral infection and preventing lung epithelial cell damage through the degradation of p65 and inhibition of the production of inflammatory cytokines.

1. Introduction

Viral infections such as H1N1 influenza, severe acute respiratory syndrome coronavirus (SARS-CoV), Middle East respiratory syndrome (MERS), and SARS-CoV-2, which is responsible for the recent coronavirus disease-19 (COVID-19), all share an important common feature. This feature is acute respiratory distress syndrome (ARDS), which can cause severe diffuse alveolar damage to the alveoli in the lungs [1–6]. Alveolar damage is accompanied by an excessive inflammatory response, which is strongly associated with increased mortality rates and severe long-term complications following recovery [7–9]. One of the hallmarks of alveolar damage is an increase in the levels of interleukin-8 (IL-8). IL-8 is produced primarily by neutrophils, but can also be found in injured lung epithelial cells [10,11]. IL-8 is a potent neutrophil chemotactic factor that plays an important role in both physiological and inflammatory conditions. Sustained expression of IL-8 contributes to an inflammatory response that can be both beneficial and potentially dangerous for patients with lung disease. This is because IL-8 binds to

Abbreviations: ANOVA, analysis of variance; ARDS, acute respiratory distress syndrome; AQ, amodiaquine; COVID-19, coronavirus disease-2019; CQ, chloroquine; FN, fibronectin; IL, interleukin; IP, intraperitoneal injection; IT, intratracheal instillation; KO, knockout; LPS, lipopolysaccharides; MERS, Middle East respiratory syndrome; MPoMA, *N*-4-(4-methoxyphenoxy-3-methylphenyl)-*N*-methylacetamide; P65, nuclear factor-kB p65; T-bet, T-box protein expressed in T cells.

* Correspondence to: Ewha Womans University, A212 Pharmacy Building, 52 Ewhayeodae-Gil, Seodaemun-Gu, Seoul 03760, Republic of Korea.
** Correspondence to: Ewha Womans University, C206 Science Building, 52 Ewhayeodae-Gil, Seodaemun-Gu, Seoul 03760, Republic of Korea.
E-mail addresses: yunjpark21@ewha.ac.kr (Y. Park), eshwang@ewha.ac.kr (E.S. Hwang).
[1] https://orcid.org/0009-0003-8361-6109
[2] http://orcid.org/0009-0003-2116-6966
[3] https://orcid.org/0009-0001-4740-4219
[4] https://orcid.org/0000-0003-0802-6398
[5] https://orcid.org/0000-0003-2166-7712
[6] http://orcid.org/0000-0001-8508-3666

https://doi.org/10.1016/j.biopha.2024.116674
Received 13 February 2024; Received in revised form 20 April 2024; Accepted 29 April 2024
Available online 4 May 2024
0753-3322/© 2024 The Authors. Published by Elsevier Masson SAS. This is an open access article under the CC BY-NC license (http://creativecommons.org/licenses/by-nc/4.0/).

the CXC chemokine receptors, CXCR1 and CXCR2, triggering an inflammatory response that protects host cells from pathogen-induced cell damage [12,13]. However, persistent expression of IL-8 in the bronchial epithelium can lead to higher numbers of neutrophils, increased neutrophil maturation and activation, and persistent chemotaxis, eventually leading to airway remodeling and dysfunctions such as hyperinflammation, mucus hypersecretion, and fibrosis [10,11,14]. Dysregulated IL-8/CXCR signaling has been identified as a possible cause of immunopathological lung injury due to the dangerous positive feedback loop of neutrophil activation [15]. Blocking alveolar damage is crucial for preventing the spread of the virus and reducing the compliances associated with infection [16]. While there has been significant recent development of substances capable of blocking viral infection, there has been relatively little development of other drugs capable of directly treating or protecting against IL-8-induced alveolar damage [17–21].

Lung epithelial cell injury can be caused by bacterial infection, exposure to bacterial lipopolysaccharides (LPS), and exposure to harmful substances in the air, such as cigarette smoke and asbestos [22,23]. Drug-induced lung toxicity has also been reported following the administration of toxic therapeutic drugs such as bleomycin or amiodarone [24–26]. Inhalation of the anticancer drug bleomycin can lead to severe inflammation of lung tissue and pulmonary fibrosis, which is characterized by an abnormal accumulation of collagen and fibronectin [27]. In addition, inadvertent overdose use or long-term administration of low doses of amodiaquine (AQ), used to treat malaria infection, can result in severe liver toxicity, causing a systemic inflammatory response and abnormalities in lung tissue, including pulmonary embolism or stenosis [28–30]. Lung injury is often accompanied by a severe inflammatory response, including marked increases in the production of IL-1β, IL-6, and IL-8 [31–34].

In this study, we aimed to identify small molecules that can inhibit both viral spike binding to the cell membrane and prevent drug-induced lung epithelial cell damage. We also aimed to evaluate the protective effects of small molecules against lung injury *in vivo*.

2. Results

2.1. Establishment of an in vitro model of lung epithelial cell injury

An *in vitro* model of lung epithelial cell injury was established by treating normal human lung epithelial BEAS-2B cells with different concentrations of the antimalarial drugs AQ and chloroquine (CQ). At concentrations above 20 μM, both AQ and CQ reduced cell viability, causing cytotoxicity (Fig. 1**A**). However, AQ and CQ at a concentration of 50 μM induced a significant increase in the expression of the pro-inflammatory cytokine IL-6 (Fig. 1**B**). We also found that the production of the lung epithelial cell-specific cytokine IL-8 was increased by treatment with 50 μM of AQ and CQ, with AQ increasing IL-8 more potently than CQ (Fig. 1**C**). Furthermore, the expression of epithelial-derived fibronectin was increased in response to 50 μM of AQ, not CQ, with AQ showing greater production than CQ (Fig. 1**D**). Therefore, we have successfully established an *in vitro* model of lung epithelial cell injury, which was verified in BEAS-2B cells after treatment with 50 μM of AQ.

2.2. Chemical synthesis and structural validation of synthetic antiviral compound derivatives

We synthesized a group of diphenyl ether derivatives with the potential to inhibit viral infection and attempted to identify compounds that can reduce lung epithelial cell damage. To create these derivatives, we used Williamson ether synthesis of 4-(trifluoromethoxy)phenol (**1a**), 4-(trifluoromethyl)phenol (**1b**), 4-methoxyphenol (**1c**) or 4-fluorophenol (**1d**) with 2-fluoro-5-nitrotoluene and generated the corresponding diphenyl ethers **2a-d** with yields of 82%-100%. Subsequent Bechamp reduction of the nitro group present on the diphenyl ethers **2a-d** resulted in the production of the corresponding amines **3a-d** at excellent yields

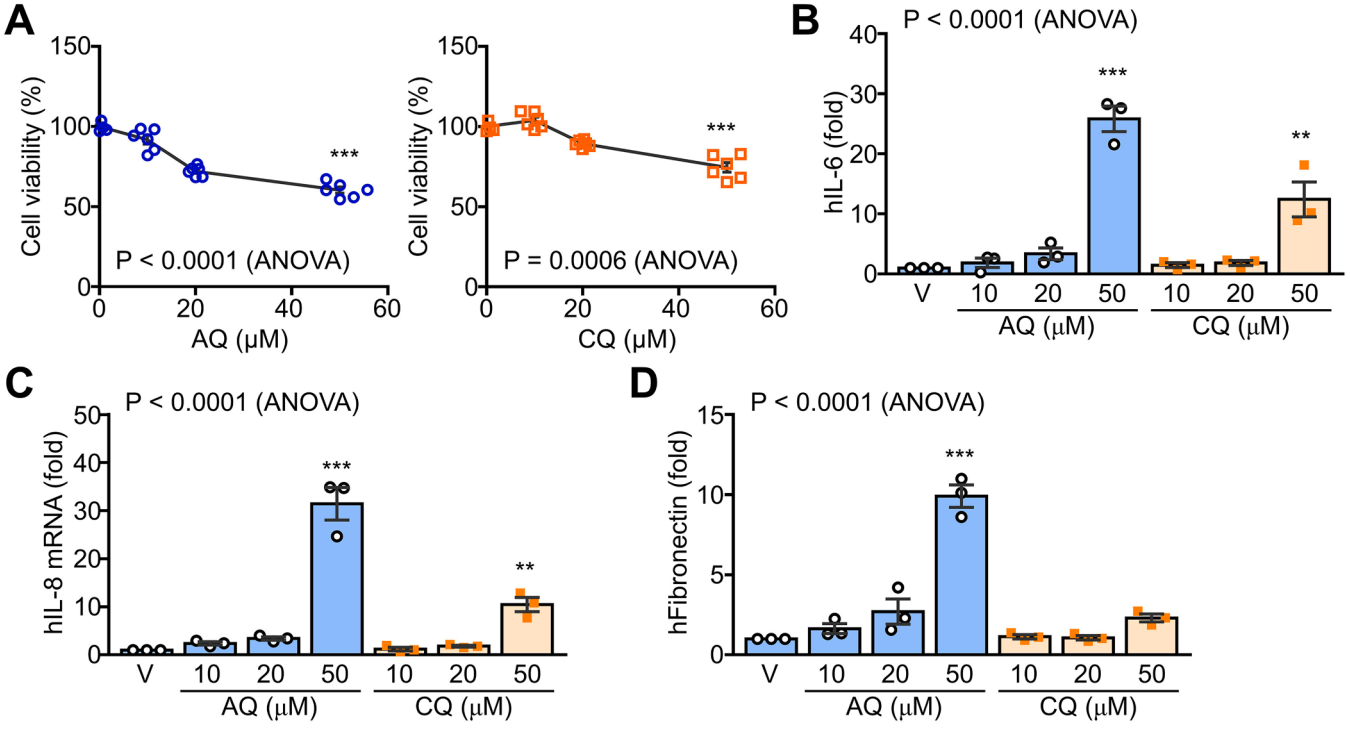


Fig. 1. Establishment of an *in vitro* model of lung epithelial cell injury. Normal lung epithelial BEAS-2B cells were treated with vehicle, AQ, or CQ for 24 h and subjected to cell viability assays and quantitative real-time PCR analysis. (**A**) Cytotoxic effects of AQ and CQ on cell viability of BEAS-2B cells. (**B-D**) Total RNA was prepared from BEAS-2B cells and the relative transcripts of hIL-6 (**B**), hIL-8 (**C**), and hfibronectin (**D**) were quantified. Data represent the mean ± SEM of at least three independent experiments. **P < 0.005; ***P < 0.0005 by ANOVA with Tukey's HSD post-hoc test.

ranging from 96% to 99%. We further subjected the compounds **3a-d** to reductive alkylation by paraformaldehyde, which generated the corresponding dimethylamines **4a-d** (yield: 82%-95%). In parallel, we also induced amine acetylation of the compounds **3a-d** with acetyl chloride to generate compounds **5a-d** (yield: 86%-96%) and subsequently reacted them with methyl iodide to give the corresponding *N*-methyl acetamides **6a-d** (yield: 80%-97%). Finally, we prepared compounds **7a-d** by reacting amines **3a-d** with succinyl anhydride, with relative yields ranging from 93% to 99% (Fig. 2**A**). All compounds were purified by column chromatography, and their structures were confirmed by NMR spectrometry (Fig. 2**B** and Supplementary Information). We then tested the cytotoxicity of all synthetic compounds in BEAS-2B cells and found that compounds **6a** and **6b** were cytotoxic and reduced cell viability. However, the other synthetic compounds had no significant effect on cell viability, increasing their potential as beneficial compounds (Fig. 2**C**).

2.3. Identification of compounds with antiviral and cytoprotective potential

We then investigated the potential inhibitory effects of the synthesized compounds on the binding of the viral spike protein to cells. To do this, we established cell lines (hACE2/HEK-293T and hACE2/BEAS-2B) that overexpress human angiotensin-converting enzyme 2 (hACE2), a known cell membrane receptor for SARS-CoV-2 and measured the binding of a fluorescently labeled viral spike protein. We found that spike protein binding was approximately 40% for hACE2/HEK-293T cells and that spike protein binding to the cells was significantly reduced by treatment with compounds **4a**, **4c**, and **6c**. Furthermore, approximately 15% of hACE2/BEAS-2B cells appeared to bind spike proteins, which was significantly reduced by **4a**, **5a**, **5b**, **6a**, and **6c** (Fig. 3**A**). These results suggest that compounds **4a** and **6c** have common effective antiviral potential. We then analyzed the effects of these compounds on IL-8 production by AQ-injured lung epithelial cells. Compounds **5a**, **6a**, **6b**, **6c**, **6d**, and **7a** significantly reduced AQ-induced IL-8 production, with compound **6c** being the most potent in reducing IL-8 production (Fig. 3**B**). Therefore, compound **6c** is proposed to exert both antiviral activity and protective effects against lung epithelial cell injury without toxicity to normal cells.

2.4. Dose-dependent suppression of IL-8 and pro-inflammatory cytokines by MPoMA

Compound **6c** is *N*-(4-(4-methoxyphenoxy)-3-methylphenyl)-*N*-methylacetamide, which we will refer to as MPoMA in the following experiments (Fig. 4**A**). As shown in Fig. 1A, 50 μM of AQ induced damage to lung epithelial cells, resulting in reduced cell viability. Treatment of BEAS-2B with MPoMA in the presence or absence of AQ did not cause cell damage at increasing concentrations (Fig. 4**B**). Interestingly, AQ treatment induced cell shrinkage in BEAS-2B cells, changing their shape to elongated. Co-treatment of MPoMA with AQ blocked AQ-induced cell shrinkage, restoring them to their standard shape (Fig. 4**C**). MPoMA also reduced IL-8 production, which was increased by AQ treatment in a concentration-dependent manner. However, MPoMA did not affect basal IL-8 levels in the absence of AQ (Fig. 4**D**). Additionally, we found that MPoMA treatment reduced the production of IL-6 and IL-1β in AQ-injured lung epithelial cells, as well as fibronectin, a hallmark of pulmonary fibrosis (Fig. 4**E**). Similarly, MPoMA also reduced IL-8 production, which was increased by CQ treatment (Fig. 4**F**). Our data demonstrate that MPoMA effectively inhibits the production of pro-inflammatory cytokines and prevents cell morphological changes in AQ-injured lung epithelial cells.

2.5. Inhibition of the transcriptional activity of nuclear factor-kB (NF-kB)/p65 by MPoMA

To understand the underlying mechanism of inhibition of pro-inflammatory cytokines and IL-8 by MPoMA, we sought to determine

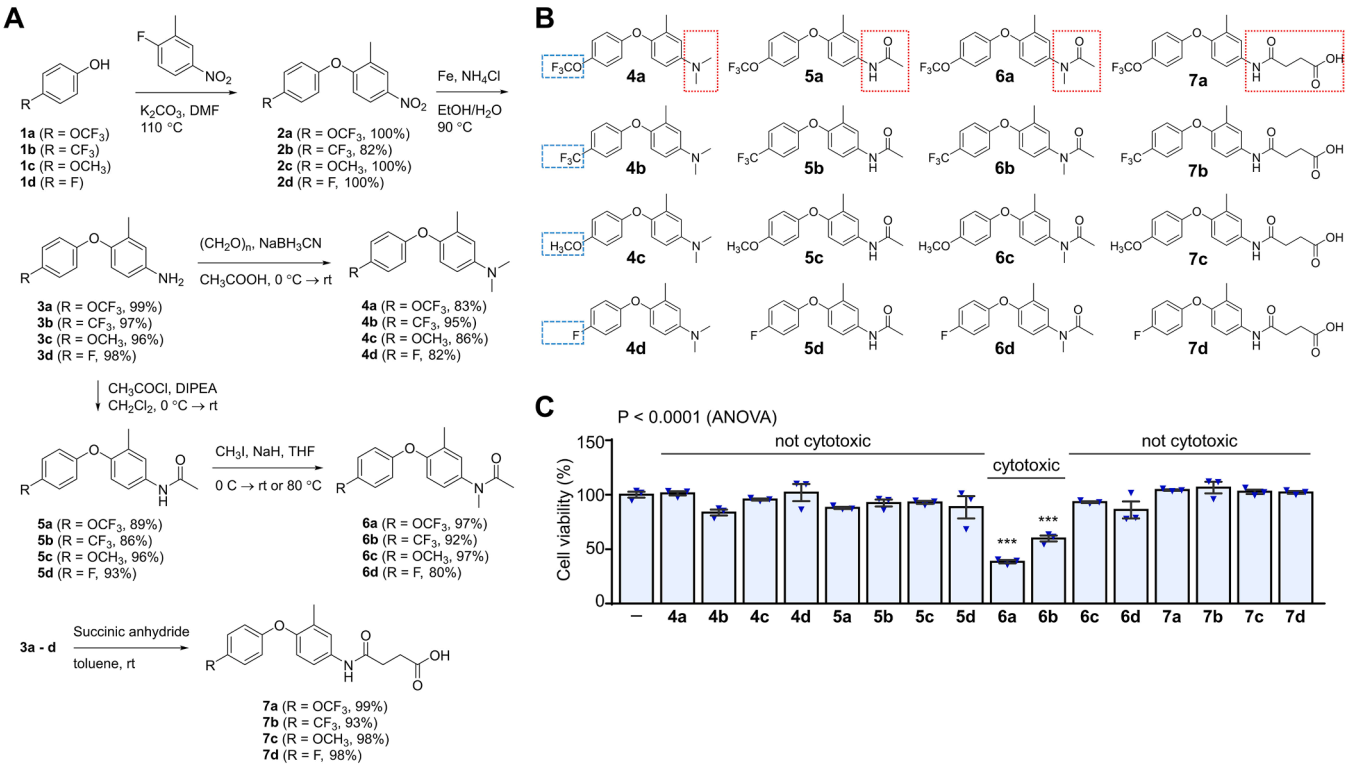


Fig. 2. Synthetic procedures and structures of diphenyl ether derivatives. (**A**) Synthetic procedures for diphenyl ether derivatives. (**B**) Structures of the synthetic diphenyl ether derivatives. (**C**) Effects of diphenyl ether derivatives on the viability of BEAS-2B cells. ***P < 0.0001 by ANOVA with Tukey's HSD post-hoc test.

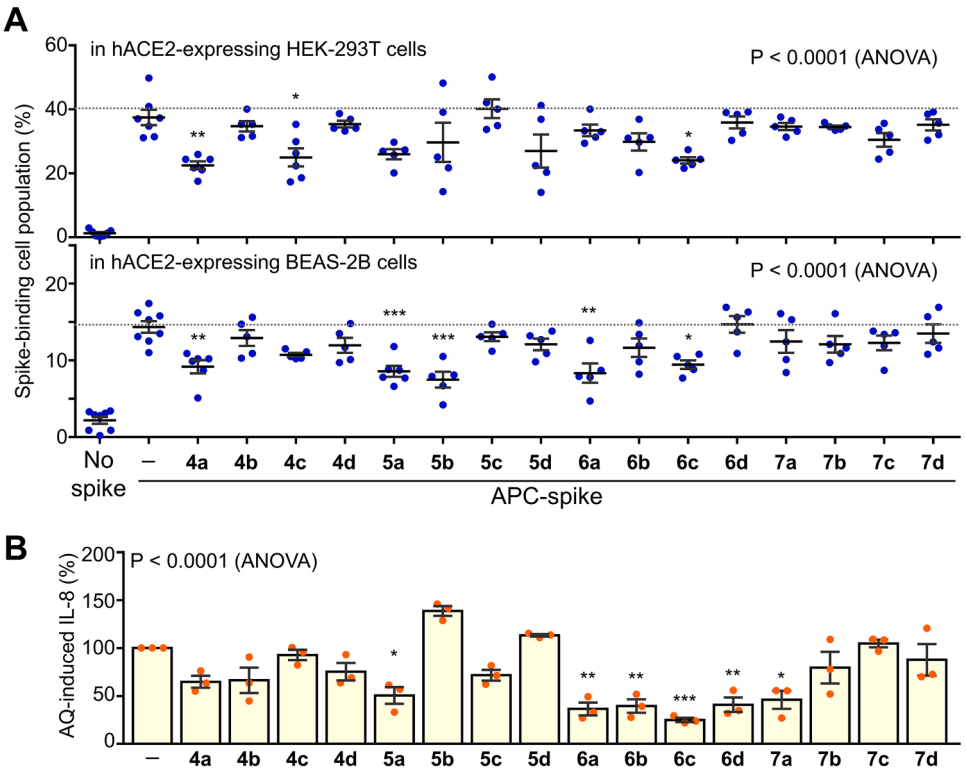


Fig. 3. Evaluation of the inhibitory effects of diphenyl ether derivatives on virus binding to the cell membranes and IL-8 production. (**A**) hACE2-HEK 293 T (top) and hACE/BEAS-2B (bottom) cells were incubated with fluorescence-labeled SARS-CoV-2 spike proteins in the presence of diphenyl ether derivatives. Spike-binding cell populations were analyzed by flow cytometry and CellQuest analysis. (**B**) BEAS-2B cells were incubated with diphenyl ether derivatives in the presence of AQ for 24 h. The inhibitory activity of diphenyl ether derivatives on IL-8 production by AQ-treated BEAS-2B cells was determined by comparison with the vehicle control. Data are the mean ± SEM of three independent experiments. *P < 0.05; **P < 0.005; ***P < 0.0005 by ANOVA with Tukey's HSD post-hoc test.

whether p65, a key regulator of pro-inflammatory cytokine production, could be modulated by MPoMA. AQ treatment appeared to increase the expression of p65 in BEAS-2B cells and also increased IL-8 promoter activity (Fig. 5**A** and **B**). However, MPoMA treatment led to a dose-dependent decrease in AQ-induced IL-8 promoter activity, which we confirmed with an NF-kB-luc reporter gene assay (Fig. 5**B**). Furthermore, when we introduced p65 expression in highly transfectable HEK-293T cells, both IL-8 promoter and NF-kB reporter activities were strongly increased by p65 overexpression. However, these effects were significantly decreased by treatment with MPoMA (Fig. 5**C**). These results indicate that MPoMA inhibits the expression of pro-inflammatory cytokines and IL-8 by inhibiting the transcriptional activity of p65, which is increased by AQ.

2.6. *MPoMA-induced proteasomal degradation of p65*

Since MPoMA inhibited p65-mediated transcription of pro-inflammatory cytokines, we next investigated whether MPoMA directly affects the expression of p65. We found that the relative transcript levels of p65 were not affected by MPoMA in AQ-treated BEAS-2B cells. However, the p65 protein level decreased by MPoMA in a dose-dependent manner (Fig. 6**A** and **B**). Immunofluorescence staining further showed that intracellular p65 expression was reduced by MPoMA treatment (Fig. 6**C**), indicating that the regulation of p65 by MPoMA was at the protein level, rather than the transcript level. We then assessed whether MPoMA induced the proteasomal degradation of p65 by treating cells with the proteasomal inhibitor MG132. The MPoMA-mediated decrease in intracellular p65 levels was increased by the addition of MG132 (Fig. 6**D**). Furthermore, immunoblot analysis confirmed that the p65 protein, which was decreased by MPoMA treatment in the presence of CHX, was increased following the addition of MG132 (Fig. 6**E**). Thus, we suggest that MPoMA induces proteasomal degradation of the p65 protein, leading to a reduction in its intracellular levels.

2.7. *In vivo protective effect of MPoMA against acute lung injury*

Having shown that MPoMA inhibits the production of IL-8 and pro-inflammatory cytokines in lung epithelial cells injured by AQ treatment *in vitro*, we sought to verify its anti-inflammatory and protective effects against lung injury *in vivo*. Mice were injected intraperitoneally with MPoMA for 7 days and subjected to intratracheal instillation of LPS, followed by lung analysis. As shown by H&E staining, intratracheal injection of LPS caused severe lung inflammation and injury, and MPoMA treatment effectively attenuated LPS-induced lung injury (Fig. 7**A**). Furthermore, the pro-inflammatory cytokines IL-6 and IL-1β, epithelial cell-derived IL-8, and fibrosis-associated fibronectin were all significantly reduced in MPoMA-treated lung tissue (Fig. 7**B**). Consistent with reduced inflammatory cytokines, the expression of surfactant protein-C (SP-C), a lung epithelial cell marker [35], was decreased in inflammatory lung tissue; however, SP-C expression was increased in a dose-dependent manner by treatment with MPoMA. At the same time, the infiltration of CD11b-expressing macrophages into the lung was significantly reduced by MPoMA [36] (Fig. 7**C**). To further validate the protective role of MPoMA against lung injury, we used T-bet knockout (KO) mice, which are reported to lack a T helper 1-mediated immune response and are susceptible to pathogenic lung inflammation. T-bet KO mice were injected intraperitoneally with MPoMA for 3 days and analyzed 6 hours after intraperitoneal injection of LPS. Intraperitoneal LPS injection caused severe lung inflammation in T-bet KO mice, and MPoMA pre-treatment sufficiently blocked the inflammation and protected airway epithelial cells against lung injury (Fig. 7**D**). At the same

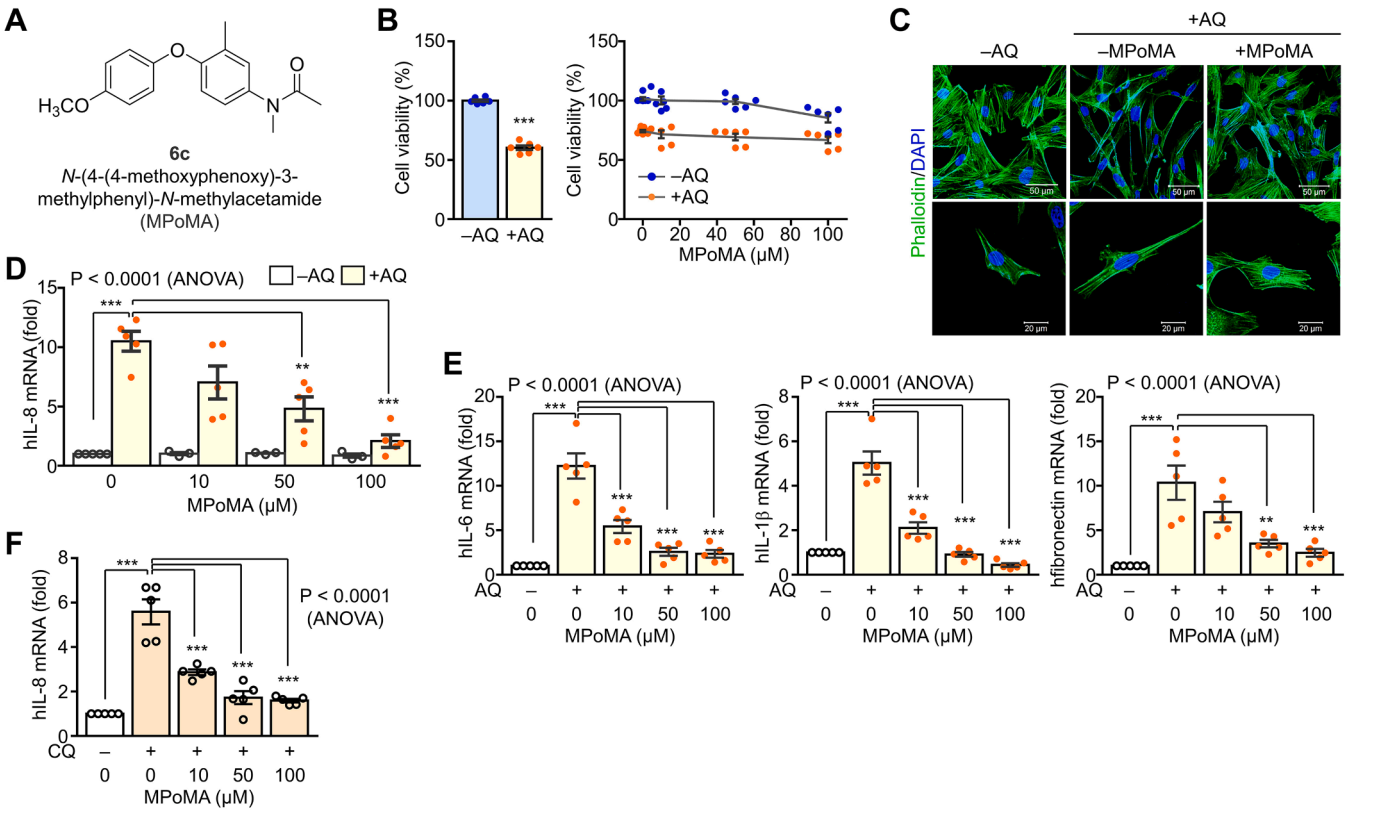


Fig. 4. Dose-dependent suppression of inflammatory cytokines by MPoMA. (**A**) Structure of MPoMA (**6c**). (**B**) BEAS-2B cells were incubated with different concentrations of MPoMA in the presence or absence of AQ (50 μM) for 24 h. Cytotoxic activity of MPoMA was determined in BEAS-2B cells. (**C**) BEAS-2B cells were treated with AQ (50 μM) in the presence or absence of MPoMA (100 μM), followed by Phalloidin staining. (**D-E**) Cells were incubated with different concentrations of MPoMA with or without AQ for 24 h and subjected to RNA extraction and quantitative real-time PCR analysis to measure the transcript of hIL-8 (**D**), hIL-6, hIL-1β, and hfibronectin (**E**). (**F**) BEAS-2B cells were treated separately with CQ (50 μM) and MPoMA (10, 50, and 100 μM) for 24 h and hIL-8 mRNA levels were then measured. *P < 0.05; **P < 0.005; ***P < 0.0005 by ANOVA with Tukey's HSD post-hoc test.

time, IL-1β production in the spleen, which was increased by LPS injection, was also significantly reduced by pre-treatment with MPoMA (Fig. 7**E**), indicating the potent anti-inflammatory and protective effects of MPoMA against LPS-induced lung injury *in vivo*.

3. Discussion

Here, we reported the establishment of an *in vitro* assay system to identify small molecules capable of inhibiting viral infection by interfering with the binding of the viral spike protein to the cell membrane and preventing AQ-induced lung epithelial cell damage. We then evaluated the inhibitory activities of various small molecules and found that MPoMA, a synthetic small molecule capable of inhibiting viral infection, efficiently inhibited the expression of IL-8, pro-inflammatory IL-1β and IL-6, and fibronectin by inducing p65 protein degradation, thereby protecting against lung epithelial cell injury *in vitro* and *in vivo*.

MPoMA has a naturally occurring diphenyl ether moiety that has been of interest in medicinal chemistry. Based on scaffold analysis and bioactivity analysis reported over 17 years (1998–2014), the diphenyl ether scaffold was the second most common moiety, after biphenyl, among 764 scaffolds by cumulative count. Moreover, this moiety is currently being used for drug development against cancer, inflammation, and microbial infection [37,38]. Diphenyl ether and its naturally-occurring derivatives are predominantly found in the marine environment, and structurally diverse derivatives have been isolated from marine sponges, macro- and microalgae, fungi, and sea slugs [39–42] and have also been reported in higher marine animals, including turtles [43,44].

Diphenyl ether derivatives have shown a variety of biological activities, including cytotoxicity, antiviral, antibacterial, cell shape elongation, and peroxidizing activity [45–49]. Recently, a diphenyl ether-containing small molecule has been identified to play an inhibitory role in the interaction between programmed cell death-1 (PD-1) and programmed cell death-ligand 1 (PD-L1), acting as an alternative to existing immune checkpoint blockers [50]. In addition, several drugs containing a diphenyl ether moiety have already been developed and used to combat a variety of diseases, including cancers and infections. Examples include ibrutinib and sorafenib, used for the treatment of leukemia and advanced kidney cancer; nimesulide, used as a non-steroidal anti-inflammatory drug; difenoconazole and flufenoxuron, used as fungicides and insect growth regulators; and toltrazuril, prescribed as an anticoccidial agent [38,51–53].

MPoMA can protect against or treat lung injury due to its efficacy in inhibiting viral infection and reducing AQ-induced lung epithelial cell damage. To further develop MPoMA as a therapeutic drug for controlling lung epithelial cell injury caused by infection, air pollution, and drug administration, the toxicity and stability of MPoMA should be evaluated in greater depth in the future. Moreover, further research is needed to determine whether it also exerts other biological functions within cells.

4. Materials and methods

4.1. Materials

AQ, CQ, MG132, and LPS were purchased from Sigma-Aldrich (St. Louis, MO, USA). All compounds reported here, including MPoMA, were synthesized and validated according to the procedures described in the

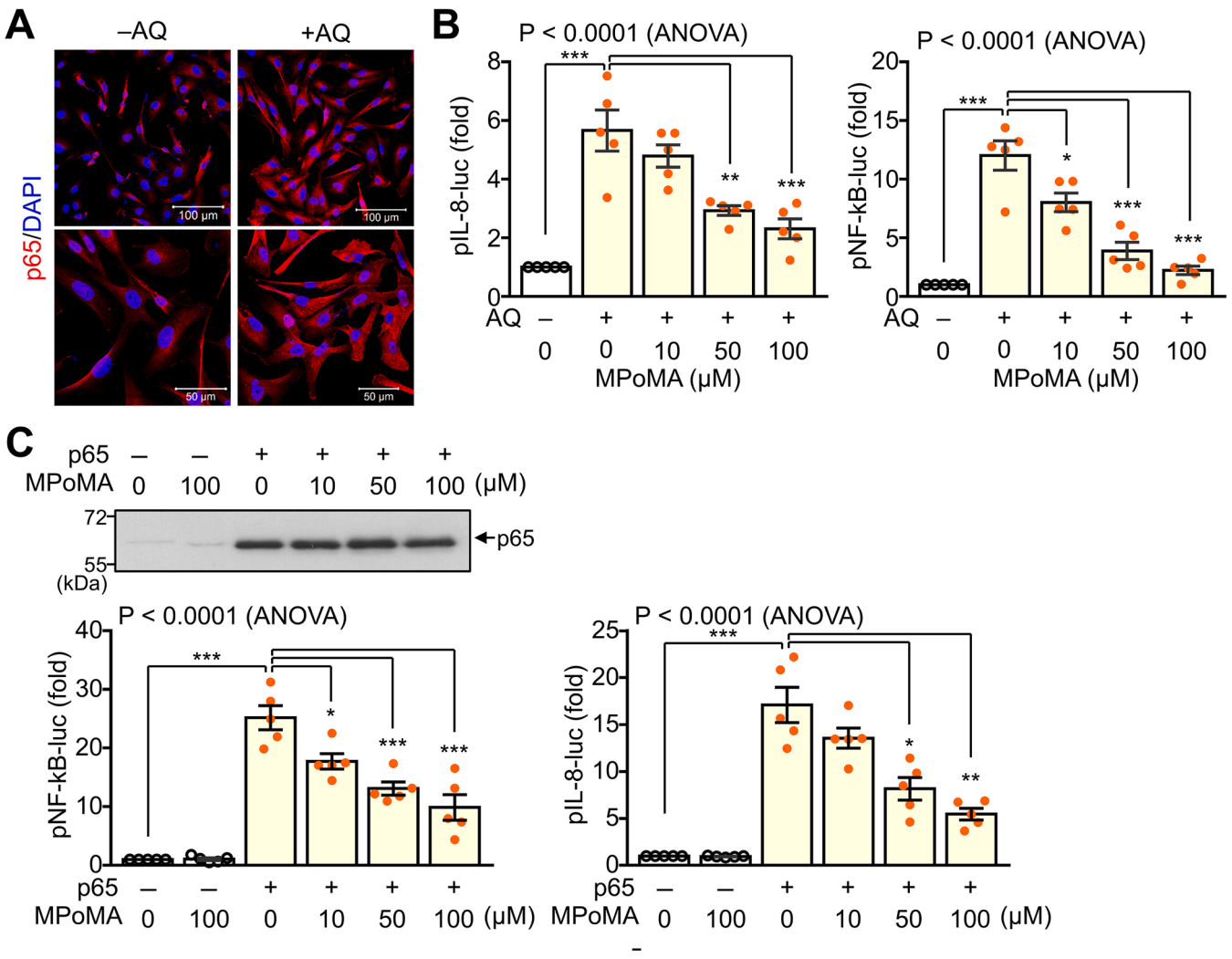


Fig. 5. Inhibition of NF-kB activity by MPoMA. (**A**) Immunofluorescence staining of p65 in BEAS-2B cells treated with either vehicle or AQ. (**B**) BEAS-2B cells were transfected with the reporter genes NF-kB-luc and pIL-8-luc and then treated with MPoMA and AQ for an additional 24 h, followed by a reporter gene assay. (**C**) HEK-293T cells were transfected with the reporter genes NF-kB-luc and pIL-8-luc together with a p65 expression vector and then incubated with MPoMA for 24 h. Subsequently, cells were subjected to immunoblotting and a reporter assay. Data are expressed as the mean ± SEM (n = 5) and were statistically analyzed by ANOVA with Tukey's HSD post-hoc test.

Supplementary Information. Synthetic compounds with 98% purity were used for all *in vitro* and *in vivo* experiments.

4.2. Cell culture and cell viability assays

Human lung epithelial BEAS-2B cells (ATCC CRL-3588, Manassas, VA, USA) were cultured in DMEM supplemented with 10% FBS and were then treated with different concentrations of AQ, CQ, or synthetic compounds for 24 h. Subsequently, cytotoxicity or cell viability was determined by incubation with EZ-Cytox reagent for 30 min, with all procedures performed according to the manufacturer's instructions (EZ-Cytox Cell Viability Assay Kit, DoGenBio, Seoul, Korea). Optical density was determined using a microplate reader (Molecular Devices, Sunnyvale, CA, USA) at the Ewha Fluorescence Imaging Core Center.

4.3. Quantitative real-time polymerase chain reaction (PCR)

BEAS-2B cells were incubated with different concentrations of compounds for 24 h, then harvested for RNA extraction using TRIzol reagent (Thermo Fischer Scientific, Carlsbad, CA, USA). Mouse lung tissue samples were lysed in TRIzol reagent for total RNA isolation, after which total RNA was subjected to reverse transcription and quantitative real-time PCR analysis using Thunderbird SYBR qPCR Mix (Toyobo, Osaka, Japan) and a Step One Plus real-time PCR system (Applied Biosystems, Carlsbad, CA, USA). The relative transcript levels of genes were calculated after normalization with the Ct values of the hActin gene. The specific human gene primer sets used were as follows: hIL-8, 5′-aggtgcagttttgccaag-3′, 5′-acttctccacaaccctctg-3′; hIL-6, 5′-tcctgatccagttcctgcag-3′, 5′-aagagccctcaggctggactg-3′; hIL-1β, 5′-aatctgtacctgtcctgcgtg-3′, 5′-tcccaggaagacgggcatg-3′; hfibronectin, 5′-tgggcaactctgtcaac-3′, 5′-aacacgttgcctcatgaggg-3′; hActin, 5′-catgtacgttgctatccaggc-3′, 5′-ctccttaatgtcacgcacgat-3′. The mouse specific primer sets used as follows: IL-6, 5′-accacttcacaagtcggagg-3′, 5′-tccaggtagctatggtactcc-3′; IL-1β, 5′-caaccaacaagtgatattctccat-3′, 5′-gatccacactctccagctgca-3′; IL-8, 5′-gatgctccatgggtgaagg-3′, 5′-tctcccgaattggaaaggg-3′; fibronectin, 5′-gtgacaactgccgtagacc-3′, 5′-ggtagagagacacttgtaggg-3′; actin, 5′-caccctgtgctgctcaccgag-3′, 5′-accgctcgttgccaatagtga-3′.

4.4. Cell-based spike-hACE2 binding inhibition assays

BEAS-2B and HEK-293T cells were maintained in DMEM with 10% FBS and transfected with pCMV3-human ACE2-Flag plasmid DNA, followed by selection in the presence of hygromycin B (Sigma-Aldrich). Next, hACE2-BEAS-2B cells and hACE2-HEK293T cells, which

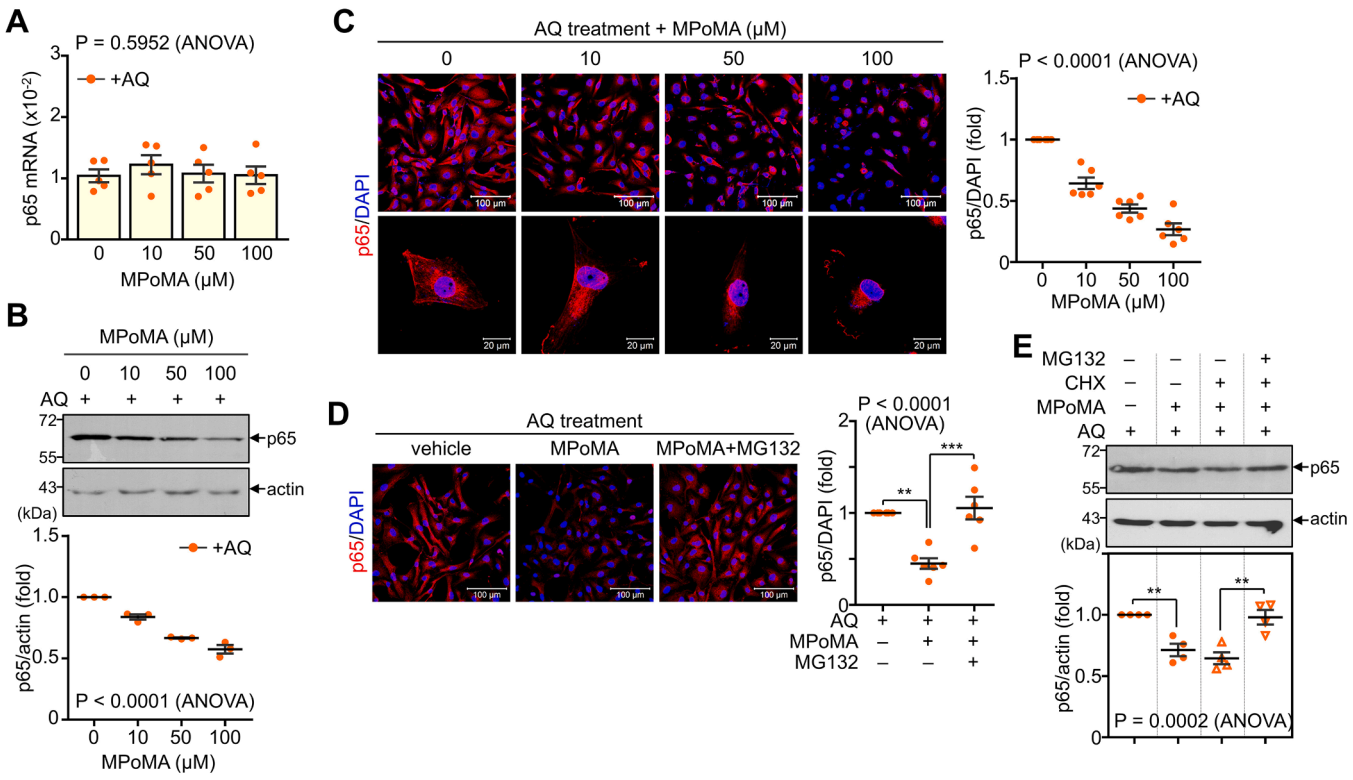


Fig. 6. Proteasomal degradation of p65 by MPoMA. BEAS-2B cells were incubated with MPoMA with AQ (50 μM) for 24 h and harvested for RNA and protein analysis and immunofluorescence staining. (**A**) Quantitative analysis of p65 transcripts in AQ-treated BEAS-2B cells. n = 5. (**B**) Protein extracts were harvested and subjected to immunoblotting analysis (n = 3). Protein band intensity was quantified using the ImageJ software (NIH). (**C**) Cells were fixed and stained with p65 antibody for immunofluorescence staining and subsequent quantitative analysis (n = 6). Immunofluorescence was quantified using the ImageJ software. (**D-E**) BEAS-2B cells were incubated with either vehicle or MPoMA (100 μM) in the presence of AQ and additionally treated with MG132 for 4 h and subjected to immunofluorescence staining (**D**, n = 6) and immunoblotting analysis (**E**, n = 4). **P < 0.005; ***P < 0.0005 by ANOVA. Data are expressed as the mean ± SEM.

overexpress human ACE2, were then established and subjected to spike binding assays. Briefly, stable cells were incubated with or without 100 ng of biotinylated SARS-CoV-2 spike protein in the absence or presence of synthetic compounds at 37 ℃ for 1 h. Cells were then incubated with streptavidin-APC on ice for 20 min, followed by flow cytometry analysis using a BD FACS Caliber (BD Biosciences, San Jose, CA, USA). Finally, cell populations were quantitatively analyzed using the CellQuest software (BD Biosciences).

4.5. Immunofluorescence staining

For immunofluorescence staining, BEAS-2B cells were plated on poly-L-lysine-coated glass coverslips (Marienfeld, Lauda-Königshofen, Germany) and were incubated with different concentrations of MPoMA in the presence or absence of AQ (50 μg/mL) for 24 h. Cells were then fixed and subjected to staining with antibodies against NF-kB p65 or Phalloidin staining (Alexa Fluor 488-Phalloidin, Thermo Fischer Scientific), followed by DAPI staining (1 μg/mL, Sigma-Aldrich) and microscopic observation under a confocal laser scanning microscope (ZEISS LSM 880 with Airyscan, Oberkochen, Germany).

4.6. Hematoxylin and eosin (HE) staining and immunohistochemistry

Lung tissues were sectioned at 4 μm thickness, fixed in paraformaldehyde solution, and subjected to hematoxylin and eosin (HE, Sigma-Aldrich) staining or immunohistochemistry. Whole lung tissue images were acquired using the MoticEasyScan device (Motic, Vancouver, Canada), and image analysis was performed by separating the HE staining data into hematoxylin (blue) and eosin (red) channels. The intensity of hematoxylin-stained inflammatory nuclei was quantified and expressed as a fold relative to the intensity of the vehicle-treated control [54]. Lung tissues were observed and photographed under an upright microscope (Nikon Eclipse Ci, Nikon, Japan) equipped at the Ewha Drug Development Research Core Center. For immunohistochemistry, lung tissues were fixed and incubated with antibodies against lung epithelial cell marker SP-C and macrophage marker CD11b, followed by incubation with fluorescence-conjugated antibodies and DAPI solution (1 μg/mL, Sigma-Aldrich). Fluorescence images were obtained by observation with a confocal microscope (ZEISS).

4.7. Reporter gene assay

BEAS-2B cells were transfected with the reporter genes pIL-8-luc and NF-kB-luc, which contain NF-kB/p65-binding sites, and then treated with AQ and various amounts of MPoMA for 24 h. Highly transfectable HEK-293T cells were transfected with the p65 expression vector and the reporter genes pIL-8-luc and NF-kB-luc and incubated with MPoMA for an additional 24 h. The reporter gene RSVβ was also transfected to provide positive control of transfection efficiency. After 24 h, cells were harvested and subjected to luciferase and β-galactosidase assays (Promega, Madison, WI, USA). Luciferase reporter activity was then normalized to β-galactosidase activity and expressed as induction fold.

4.8. Immunoblot analysis

BEAS-2B cells were treated with MPoMA for 24 h and subjected to protein extraction using RIPA lysis buffer. Protein lysates were resolved by SDS-PAGE and transferred to PVDF membranes, followed by incubation with p65 antibody (Cell Signaling Technology, Danvers, MA, USA), and β-actin (Bioss, Woburn, MA, USA). The protein signal was

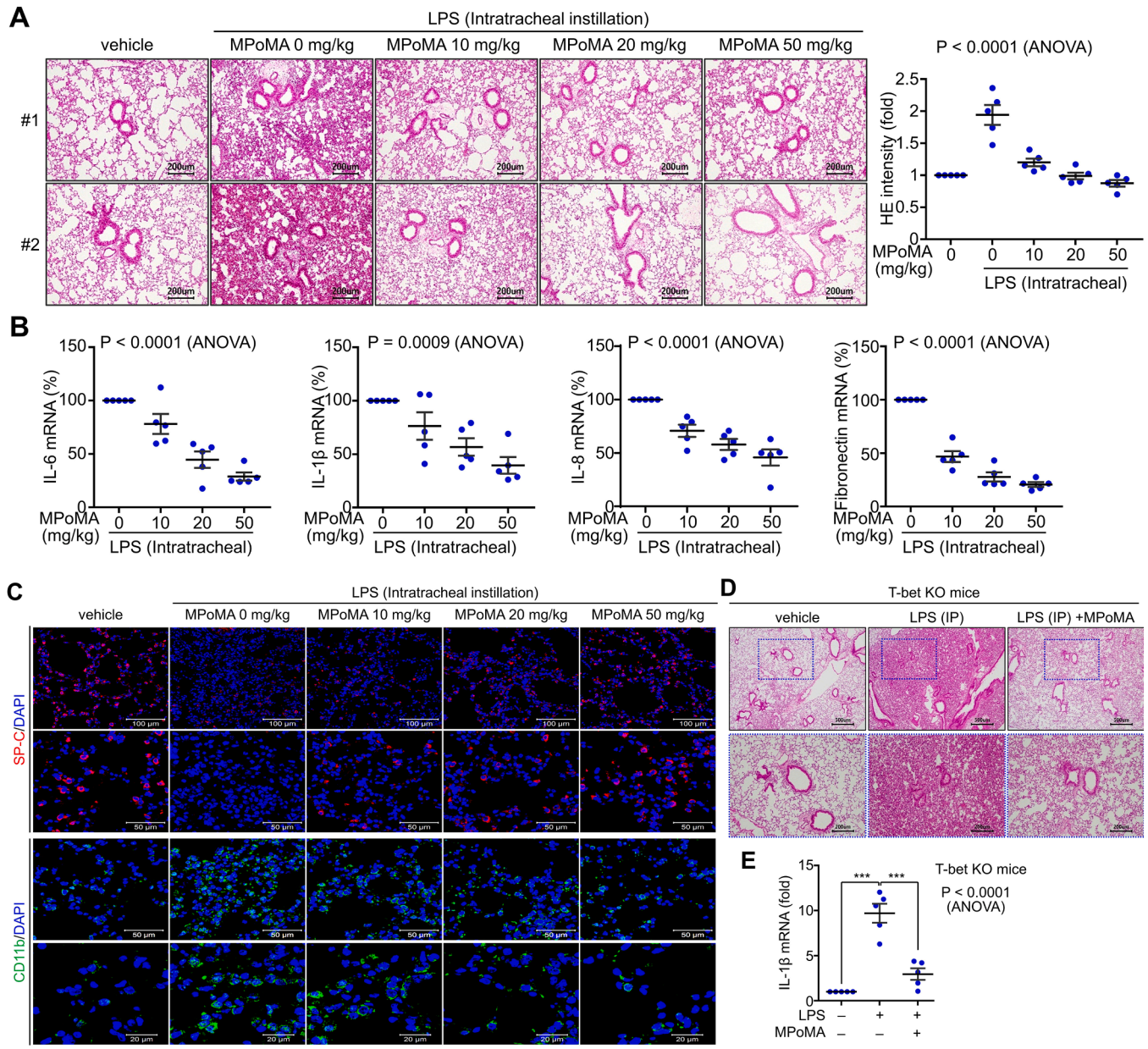


Fig. 7. ***In vivo*** **protective effect of MPoMA against acute lung injury.** (**A-B**) C57BL6 mice (male, n = 5) were injected with either vehicle or MPoMA (at 10, 20, or 50 mg/kg) for 7 consecutive days. Mice were then exposed to LPS (5 mg/kg) via intratracheal instillation overnight. Lung tissue samples were collected and subjected to HE staining and quantification (**A**). Total RNA was harvested from lung tissues and the relative transcripts of IL-6, IL-1β, IL-8, and fibronectin were analyzed by quantitative real-time PCR. (**C**) Lung tissue was subjected to immunohistochemistry analysis with antibodies against SP-C and CD11b as well as DAPI staining. (**D-E**) T-bet KO mice (n = 5), which are susceptible to infection and inflammation, were pre-treated with MPoMA (20 mg/kg) for 3 days and injected with LPS for 6 h. Lung tissue samples were collected from the mice and subjected to HE staining (**D**). Spleen samples were collected and IL-1β transcripts were analyzed in the spleen by reverse transcription and quantitative real-time PCR (**E**). Representative images are shown, and data represent the mean ± SEM. ANOVA with Tukey's HSD post-hoc test.

visualized after incubation with the ECL detection reagent (Cytiva, Marlborough, MA, USA).

4.9. Acute lung injury animal model

For *in vivo* efficacy testing, C57BL6/J mice (male, 8–10 weeks old) were pretreated with different doses of MPoMA (0, 10, 20, or 50 mg/kg) daily for 7 consecutive days via intraperitoneal injection. The mice were then exposed to LPS (5 mg/kg, intratracheal instillation) overnight. Separately, T-bet KO mice (male, 8–10 weeks old) were given MPoMA (20 mg/kg) for 3 consecutive days and injected with LPS (5 mg/kg) by intraperitoneal injection for 6 h. Lung tissue samples were harvested from all mice for further analysis. All animal experiments were conducted according to the international animal welfare guidelines and all procedures were approved by the Institutional Animal Care and Use Committee of Ewha Womans University (IACUC 19–010 and 21–072).

4.10. Statistical analysis

All experiments were performed at least three times, and all data are expressed as mean ± standard error of the mean (SEM). All statistical analysis was performed using Prism 7.0 (GraphPad Software Inc., San Diego, CA, USA). The statistical significance of mean differences was analyzed using one-way analysis of variance (ANOVA) with Tukey's

HSD post-hoc test. P values less than 0.05 from Tukey's multiple comparison test were considered to be statistically significant.

Author contributions

SL and SJY performed most experiments and JHO performed animal experiments. JSR and YP designed the synthetic strategy and performed the synthesis and purification of compounds. ESH instructed all experimental plans and prepared the manuscript for publication.

Declaration of Generative AI and AI-assisted technologies in the writing process

No declaration of generative AI and AI-assisted technologies

Funding

This work was supported by the grants of the National Research Foundation (NRF-2018R1A5A2025286 and 2020R1A2C2004679 for ESH; 2022R1I1A1A01064498 For YP; 2021R1A6C101A442 for ESH and YP) funded by the Ministry of Science and ICT.

CRediT authorship contribution statement

Suh Jin Yoon: Methodology, Investigation, Formal analysis, Data curation. **Soheun Lee:** Software, Methodology, Investigation, Data curation. **Ji Hyun Oh:** Investigation. **Yunjeong Park:** Writing – original draft, Investigation, Funding acquisition, Formal analysis, Data curation. **Jae-Sang Ryu:** Validation, Resources, Conceptualization. **Eun Sook Hwang:** Writing – review & editing, Writing – original draft, Visualization, Supervision, Project administration.

Declaration of Competing Interest

The authors declare no competing financial interests

Data Availability

No data was used for the research described in the article.

Acknowledgments

None

Appendix A. Supporting information

Supplementary data associated with this article can be found in the online version at doi:10.1016/j.biopha.2024.116674.

References

[1] P.W. Harms, L.A. Schmidt, L.B. Smith, D.W. Newton, M.A. Pletneva, L.L. Walters, S. A. Tomlins, A. Fisher-Hubbard, L.M. Napolitano, P.K. Park, M. Blaivas, J. Fantone, J.L. Myers, J.M. Jentzen, Autopsy findings in eight patients with fatal H1N1 influenza, Am. J. Clin. Pathol. 134 (2010) 27–35, https://doi.org/10.1309/AJCP35KOZSAVNQZW.

[2] K.G. Andersen, A. Rambaut, W.I. Lipkin, E.C. Holmes, R.F. Garry, The proximal origin of SARS-CoV-2, Nat. Med 26 (2020) 450–452, https://doi.org/10.1038/s41591-020-0820-9.

[3] D. Fox, What you need to know about the novel coronavirus, Nature (2020), https://doi.org/10.1038/d41586-020-00209-y.

[4] K.E. Konopka, T. Nguyen, J.M. Jentzen, O. Rayes, C.J. Schmidt, A.M. Wilson, C. F. Farver, J.L. Myers, Diffuse alveolar damage (DAD) resulting from coronavirus disease 2019 infection is morphologically indistinguishable from other causes of DAD, Histopathology 77 (2020) 570–578, https://doi.org/10.1111/his.14180.

[5] L.P. Hariri, C.M. North, A.R. Shih, R.A. Israel, J.H. Maley, J.A. Villalba, V. Vinarsky, J. Rubin, D.A. Okin, A. Sclafani, J.W. Alladina, J.W. Griffith, M. A. Gillette, Y. Raz, C.J. Richards, A.K. Wong, A. Ly, Y.P. Hung, R.R. Chivukula, C. R. Petri, T.F. Calhoun, L.N. Brenner, K.A. Hibbert, B.D. Medoff, C.C. Hardin, J. R. Stone, M. Mino-Kenudson, Lung histopathology in coronavirus disease 2019 as compared with severe acute respiratory syndrome and H1N1 influenza: a systematic review, Chest 159 (2021) 73–84, https://doi.org/10.1016/j.chest.2020.09.259.

[6] R.F. Barth, L.M. Buja, A.L. Barth, D.E. Carpenter, A.V. Parwani, A comparison of the clinical, viral, pathologic, and immunologic features of severe acute respiratory syndrome (SARS), middle east respiratory syndrome (MERS), and coronavirus 2019 (COVID-19) diseases, Arch. Pathol. Lab Med 145 (2021) 1194–1211, https://doi.org/10.5858/arpa.2020-0820-SA.

[7] L. Carsana, A. Sonzogni, A. Nasr, R.S. Rossi, A. Pellegrinelli, P. Zerbi, R. Rech, R. Colombo, S. Antinori, M. Corbellino, M. Galli, E. Catena, A. Tosoni, A. Gianatti, M. Nebuloni, Pulmonary post-mortem findings in a series of COVID-19 cases from northern Italy: a two-centre descriptive study, Lancet Infect. Dis. 20 (2020) 1135–1140, https://doi.org/10.1016/S1473-3099(20)30434-5.

[8] M. Sakka, J.M. Connors, G. Hekimian, I. Martin-Toutain, B. Crichi, I. Colmegna, D. Bonnefont-Rousselot, D. Farge, C. Frere, Association between D-Dimer levels and mortality in patients with coronavirus disease 2019 (COVID-19): a systematic review and pooled analysis, J. Med Vasc 45 (2020) 268–274, https://doi.org/10.1016/j.jdmv.2020.05.003.

[9] Z. Xu, L. Shi, Y. Wang, J. Zhang, L. Huang, C. Zhang, S. Liu, P. Zhao, H. Liu, L. Zhu, Y. Tai, C. Bai, T. Gao, J. Song, P. Xia, J. Dong, J. Zhao, F.S. Wang, Pathological findings of COVID-19 associated with acute respiratory distress syndrome, Lancet Respir. Med 8 (2020) 420–422, https://doi.org/10.1016/S2213-2600(20)30076-X.

[10] K. Matsushima, K. Morishita, T. Yoshimura, S. Lavu, Y. Kobayashi, W. Lew, E. Appella, H.F. Kung, E.J. Leonard, J.J. Oppenheim, Molecular cloning of a human monocyte-derived neutrophil chemotactic factor (MDNCF) and the induction of MDNCF mRNA by interleukin 1 and tumor necrosis factor, J. Exp. Med 167 (1988) 1883–1893, https://doi.org/10.1084/jem.167.6.1883.

[11] J.L. Simpson, S. Phipps, P.G. Gibson, Inflammatory mechanisms and treatment of obstructive airway diseases with neutrophilic bronchitis, Pharm. Ther. 124 (2009) 86–95, https://doi.org/10.1016/j.pharmthera.2009.06.004.

[12] W.E. Holmes, J. Lee, W.J. Kuang, G.C. Rice, W.I. Wood, Structure and functional expression of a human interleukin-8 receptor, Science 253 (1991) 1278–1280, https://doi.org/10.1126/science.1840701.

[13] L. Wu, N. Ruffing, X. Shi, W. Newman, D. Soler, C.R. Mackay, S. Qin, Discrete steps in binding and signaling of interleukin-8 with its receptor, J. Biol. Chem. 271 (1996) 31202–31209, https://doi.org/10.1074/jbc.271.49.31202.

[14] M.C. Cesta, M. Zippoli, C. Marsiglia, E.M. Gavioli, F. Mantelli, M. Allegretti, R. A. Balk, The role of interleukin-8 in lung inflammation and injury: implications for the management of COVID-19 and hyperinflammatory acute respiratory distress syndrome, Front Pharm. 12 (2021) 808797, https://doi.org/10.3389/fphar.2021.808797.

[15] R. Kaiser, A. Leunig, K. Pekayvaz, O. Popp, M. Joppich, V. Polewka, R. Escaig, A. Anjum, M.L. Hoffknecht, C. Gold, S. Brambs, A. Engel, S. Stockhausen, V. Knottenberg, A. Titova, M. Haji, C. Scherer, M. Muenchhoff, J.C. Hellmuth, K. Saar, B. Schubert, A. Hilgendorff, C. Schulz, S. Kaab, R. Zimmer, N. Hubner, S. Massberg, P. Mertins, L. Nicolai, K. Stark, Self-sustaining IL-8 loops drive a prothrombotic neutrophil phenotype in severe COVID-19, JCI Insight 6 (2021), https://doi.org/10.1172/jci.insight.150862.

[16] A. Mulay, B. Konda, G. Garcia Jr., C. Yao, S. Beil, J.M. Villalba, C. Koziol, C. Sen, A. Purkayastha, J.K. Kolls, D.A. Pociask, P. Pessina, J.S. de Aja, C. Garcia-de-Alba, C.F. Kim, B. Gomperts, V. Arumugaswami, B.R. Stripp, SARS-CoV-2 infection of primary human lung epithelium for COVID-19 modeling and drug discovery, Cell Rep. 35 (2021) 109055, https://doi.org/10.1016/j.celrep.2021.109055.

[17] L. Chitsike, P. Duerksen-Hughes, Keep out! SARS-CoV-2 entry inhibitors: their role and utility as COVID-19 therapeutics, Virol. J. 18 (2021) 154, https://doi.org/10.1186/s12985-021-01624-x.

[18] W.H.O.S.T. Consortium, H. Pan, R. Peto, A.M. Henao-Restrepo, M.P. Preziosi, V. Sathiyamoorthy, Q. Abdool Karim, M.M. Alejandria, C. Hernandez Garcia, M. P. Kieny, R. Malekzadeh, S. Murthy, K.S. Reddy, M. Roses Periago, P. Abi Hanna, F. Ader, A.M. Al-Bader, A. Alhasawi, E. Allum, A. Alotaibi, C.A. Alvarez-Moreno, S. Appadoo, A. Asiri, P. Aukrust, A. Barratt-Due, S. Bellani, M. Branca, H.B. C. Cappel-Porter, N. Cerrato, T.S. Chow, N. Como, J. Eustace, P.J. Garcia, S. Godbole, E. Gotuzzo, L. Griskevicius, R. Hamra, M. Hassan, M. Hassany, D. Hutton, I. Irmansyah, L. Jancoriene, J. Kirwan, S. Kumar, P. Lennon, G. Lopardo, P. Lydon, N. Magrini, T. Maguire, S. Manevska, O. Manuel, S. McGinty, M. T. Medina, M.L. Mesa Rubio, M.C. Miranda-Montoya, J. Nel, E.P. Nunes, M. Perola, A. Portoles, M.R. Rasmin, A. Raza, H. Rees, P.P.S. Reges, C.A. Rogers, K. Salami, M. I. Salvadori, N. Sinani, J.A.C. Sterne, M. Stevanovikj, E. Tacconelli, K.A. O. Tikkinen, S. Trelle, H. Zaid, J.A. Rottingen, S. Swaminathan, Repurposed Antiviral Drugs for Covid-19 - Interim WHO Solidarity Trial Results, N. Engl. J. Med 384 (2021) 497–511, https://doi.org/10.1056/NEJMoa2023184.

[19] A. Frediansyah, F. Nainu, K. Dhama, M. Mudatsir, H. Harapan, Remdesivir and its antiviral activity against COVID-19: A systematic review, Clin. Epidemiol. Glob. Health 9 (2021) 123–127, https://doi.org/10.1016/j.cegh.2020.07.011.

[20] M. Hoffmann, H. Kleine-Weber, S. Schroeder, N. Kruger, T. Herrler, S. Erichsen, T. S. Schiergens, G. Herrler, N.H. Wu, A. Nitsche, M.A. Muller, C. Drosten, S. Pohlmann, SARS-CoV-2 Cell Entry Depends on ACE2 and TMPRSS2 and Is Blocked by a Clinically Proven Protease Inhibitor, e278, Cell 181 (2020) 271–280, https://doi.org/10.1016/j.cell.2020.02.052.

[21] R.M. Meganck, R.S. Baric, Developing therapeutic approaches for twenty-first-century emerging infectious viral diseases, Nat. Med 27 (2021) 401–410, https://doi.org/10.1038/s41591-021-01282-0.

[22] D. Dreyfuss, J.D. Ricard, Acute lung injury and bacterial infection, Clin. Chest Med 26 (2005) 105–112, https://doi.org/10.1016/j.ccm.2004.10.014.

[23] J. Wong, B.E. Magun, L.J. Wood, Lung inflammation caused by inhaled toxicants: a review, Int J. Chron. Obstruct Pulmon Dis. 11 (2016) 1391–1401, https://doi.org/10.2147/COPD.S106009.
[24] B. Al-Shammari, M. Khalifa, S.A. Bakheet, M. Yasser, A Mechanistic Study on the Amiodarone-Induced Pulmonary Toxicity, Oxid. Med Cell Longev. 2016 (2016) 6265853, https://doi.org/10.1155/2016/6265853.
[25] R. Maruhashi, H. Eguchi, R. Akizuki, S. Hamada, T. Furuta, T. Matsunaga, S. Endo, K. Ichihara, A. Ikari, Chrysin enhances anticancer drug-induced toxicity mediated by the reduction of claudin-1 and 11 expression in a spheroid culture model of lung squamous cell carcinoma cells, Sci. Rep. 9 (2019) 13753, https://doi.org/10.1038/s41598-019-50276-z.
[26] H. Eguchi, Y. Yu, T. Matsunaga, Y. Yoshino, A. Ikari, Acrolein suppresses anticancer drug-induced toxicity mediated by activating claudin-1 and Nrf2 axis in a spheroid model of human lung squamous cell carcinoma cells, Toxicol. Lett. 392 (2023) 46–55, https://doi.org/10.1016/j.toxlet.2023.12.012.
[27] J.D. Williamson, L.R. Sadofsky, S.P. Hart, The pathogenesis of bleomycin-induced lung injury in animals and its applicability to human idiopathic pulmonary fibrosis, Exp. Lung Res 41 (2015) 57–73, https://doi.org/10.3109/01902148.2014.979516.
[28] F. Liu, P. Cai, I. Metushi, J. Li, T. Nakayawa, L. Vega, J. Uetrecht, Exploring an animal model of amodiaquine-induced liver injury in rats and mice, J. Immunotoxicol. 13 (2016) 694–712, https://doi.org/10.3109/1547691X.2016.1166167.
[29] K.A. Neftel, W. Woodtly, M. Schmid, P.G. Frick, J. Fehr, Amodiaquine induced agranulocytosis and liver damage, Br. Med J. Clin. Res Ed. 292 (1986) 721–723, https://doi.org/10.1136/bmj.292.6522.721.
[30] G.O. Adjei, B.Q. Goka, O.P. Rodrigues, L.C. Hoegberg, M. Alifrangis, J. Kurtzhals, Amodiaquine-associated adverse effects after inadvertent overdose and after a standard therapeutic dose, Ghana Med J. 43 (2009) 135–138, https://doi.org/10.4314/gmj.v43i3.55340.
[31] S. Kotecha, L. Wilson, A. Wangoo, M. Silverman, R.J. Shaw, Increase in interleukin (IL)-1 beta and IL-6 in bronchoalveolar lavage fluid obtained from infants with chronic lung disease of prematurity, Pedia Res 40 (1996) 250–256, https://doi.org/10.1203/00006450-199608000-00010.
[32] P. Conti, G. Ronconi, A. Caraffa, C.E. Gallenga, R. Ross, I. Frydas, S.K. Kritas, Induction of pro-inflammatory cytokines (IL-1 and IL-6) and lung inflammation by Coronavirus-19 (COVI-19 or SARS-CoV-2): anti-inflammatory strategies, J. Biol. Regul. Homeost. Agents 34 (2020) 327–331, https://doi.org/10.23812/CONTI-E.
[33] H. Chen, W. Liu, Y. Wang, D. Liu, L. Zhao, J. Yu, SARS-CoV-2 activates lung epithelial cell proinflammatory signaling and leads to immune dysregulation in COVID-19 patients, EBioMedicine 70 (2021) 103500, https://doi.org/10.1016/j.ebiom.2021.103500.
[34] J.P. Bridges, E.K. Vladar, H. Huang, R.J. Mason, Respiratory epithelial cell responses to SARS-CoV-2 in COVID-19, Thorax 77 (2022) 203–209, https://doi.org/10.1136/thoraxjnl-2021-217561.
[35] M.F. Beers, C.A. Lomax, S.J. Russo, Synthetic processing of surfactant protein C by alveolar epithelial cells. The COOH terminus of proSP-C is required for post-translational targeting and proteolysis, J. Biol. Chem. 273 (1998) 15287–15293, https://doi.org/10.1074/jbc.273.24.15287.
[36] M. Duan, D.P. Steinfort, D. Smallwood, M. Hew, W. Chen, M. Ernst, L.B. Irving, G. P. Anderson, M.L. Hibbs, CD11b immunophenotyping identifies inflammatory profiles in the mouse and human lungs, Mucosal Immunol. 9 (2016) 550–563, https://doi.org/10.1038/mi.2015.84.
[37] B. Zdrazil, R. Guha, The rise and fall of a scaffold: a trend analysis of scaffolds in the medicinal chemistry literature, J. Med Chem. 61 (2018) 4688–4703, https://doi.org/10.1021/acs.jmedchem.7b00954.
[38] T. Chen, H. Xiong, J.F. Yang, X.L. Zhu, R.Y. Qu, G.F. Yang, Diaryl ether: a privileged scaffold for drug and agrochemical discovery, J. Agric. Food Chem. 68 (2020) 9839–9877, https://doi.org/10.1021/acs.jafc.0c03369.
[39] K. Haraguchi, Y. Kato, C. Ohta, N. Koga, T. Endo, Marine sponge: a potential source for methoxylated polybrominated diphenyl ethers in the Asia-Pacific food web, J. Agric. Food Chem. 59 (2011) 13102–13109, https://doi.org/10.1021/jf203458r.
[40] G. Yang, K. Yun, V.N. Nenkep, H.D. Choi, J.S. Kang, B.W. Son, Induced production of halogenated diphenyl ethers from the marine-derived fungus Penicillium chrysogenum, Chem. Biodivers. 7 (2010) 2766–2770, https://doi.org/10.1002/cbdv.201000067.
[41] G.F. Hao, Y. Tan, N.X. Yu, G.F. Yang, Structure-activity relationships of diphenyl-ether as protoporphyrinogen oxidase inhibitors: insights from computational simulations, J. Comput. Aided Mol. Des. 25 (2011) 213–222, https://doi.org/10.1007/s10822-011-9412-6.
[42] S.G. Kini, E. Rathi, A. Kumar, V. Bhat, Potentials of diphenyl ether scaffold as a therapeutic agent: a review, Mini Rev. Med Chem. 19 (2019) 1392–1406, https://doi.org/10.2174/1389557519666190312150132.
[43] J. Melcher, D. Janussen, M.J. Garson, J. Hiebl, W. Vetter, Polybrominated hexahydroxanthene derivatives (PBHDs) and other halogenated natural products from the Mediterranean sponge Scalarispongia scalaris in marine biota, Arch. Environ. Contam. Toxicol. 52 (2007) 512–518, https://doi.org/10.1007/s00244-006-0141-0.
[44] W. Vetter, E. Stoll, M.J. Garson, S.J. Fahey, C. Gaus, J.F. Muller, Sponge halogenated natural products found at parts-per-million levels in marine mammals, Environ. Toxicol. Chem. 21 (2002) 2014–2019.
[45] P. Camilleri, K. Weaver, M.T. Clark, J.R. Bowyer, B.J. Hallahan, Some novel diphenyl ether herbicides with peroxidizing activity, J. Agric. Food Chem. 36 (1988) 1061–1063, https://doi.org/10.1021/jf00083a037.
[46] T. Bunyapaiboonsri, S. Yoiprommarat, K. Intereya, K. Kocharin, New diphenyl ethers from the insect pathogenic fungus Cordyceps sp. BCC 1861, Chem. Pharm. Bull. 55 (2007) 304–307, https://doi.org/10.1248/cpb.55.304.
[47] Z. Lu, H. Zhu, P. Fu, Y. Wang, Z. Zhang, H. Lin, P. Liu, Y. Zhuang, K. Hong, W. Zhu, Cytotoxic polyphenols from the marine-derived fungus Penicillium expansum, J. Nat. Prod. 73 (2010) 911–914, https://doi.org/10.1021/np100059m.
[48] Y. Asami, J.H. Jang, H. Oh, J.H. Sohn, J.W. Kim, D.O. Moon, O. Kwon, M. Kawatani, H. Osada, B.Y. Kim, J.S. Ahn, Violaceols function as actin inhibitors inducing cell shape elongation in fibroblast cells, Biosci. Biotechnol. Biochem 76 (2012) 1431–1437, https://doi.org/10.1271/bbb.120074.
[49] J. Xiao, J.Y. Hu, H.D. Sun, X. Zhao, W.T. Zhong, D.Z. Duan, L. Wang, X.L. Wang, Sinopestalotiollides A-D, cytotoxic diphenyl ether derivatives from plant endophytic fungus Pestalotiopsis palmarum, Bioorg. Med Chem. Lett. 28 (2018) 515–518, https://doi.org/10.1016/j.bmcl.2017.11.044.
[50] S. Shaabani, L. Gadina, E. Surmiak, Z. Wang, B. Zhang, R. Butera, T. Zarganes-Tzitzikas, I. Rodriguez, J. Kocik-Krol, K. Magiera-Mularz, L. Skalniak, A. Domling, T.A. Holak, Biphenyl ether analogs containing pomalidomide as small-molecule inhibitors of the programmed cell death-1/programmed cell death-ligand 1 interaction, Molecules 27 (2022), https://doi.org/10.3390/molecules27113454.
[51] E. Kovacs, H. Ali, R. Minorics, P. Traj, V. Resch, G. Paragi, B. Bruszel, I. Zupko, E. Mernyak, Synthesis and antiproliferative activity of steroidal diaryl ethers, Molecules 28 (2023), https://doi.org/10.3390/molecules28031196.
[52] K.D. Rainsford, N. Members of the Consensus Report Group on, Nimesulide – a multifactorial approach to inflammation and pain: scientific and clinical consensus, Curr. Med Res Opin. 22 (2006) 1161–1170, https://doi.org/10.1185/030079906×104849.
[53] Y. Ma, Y.R. Wang, Y.H. He, Y.Y. Ding, J.X. An, Z.J. Zhang, W.B. Zhao, Y.M. Hu, Y. Q. Liu, Drug repurposing strategy part 1: from approved drugs to agri-bactericides leads, J. Antibiot. 76 (2023) 27–51, https://doi.org/10.1038/s41429-022-00574-y.
[54] A. Gray, A. Wright, P. Jackson, M. Hale, D. Treanor, Quantification of histochemical stains using whole slide imaging: development of a method and demonstration of its usefulness in laboratory quality control, J. Clin. Pathol. 68 (2015) 192–199, https://doi.org/10.1136/jclinpath-2014-202526.